"Electronic Supplement"

Proc. R. Soc. A 2017 473 20170315; DOI: 10.1098/rspa.2017.0315.
Published 13 September 2017

Numerical studies of cavitation erosion on an elastic-plastic material caused by shock-induced bubble collapse

C. K. Turangan[1], G. J. Ball[2], R. Jamaluddin[3], T. G. Leighton[3,4]

[1]Department of Fluid Dynamics, Institute of High Performance Computing, Singapore 138632
[2]AtomicWeapons Establishment, Aldermaston, Reading RG7 4PR, UK
[3]Faculty of Engineering and the Environment, and [4]Institute of Sound and Vibration Research, University of Southampton, Highfield, Southampton SO17 1BJ, UK

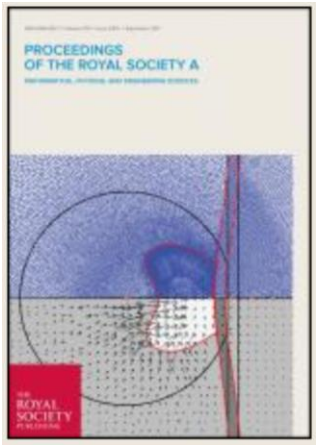

1. Introduction

Shock-induced collapse of gas-filled cavitation bubbles in liquids can result in formation and impingement of high speed jets whose velocity can reach over 1 km/s, depending on bubble size and shock strength. If the bubbles reside very close or are attached to solid walls, the velocity can reach high subsonic or even supersonic speed because of the additional compression of the bubble by the reflected shock. The jet impact on the walls imposes a high stress and strain liquid motion that leads to solid erosion and eventually a substantial damage if the number of bubbles is high. The pressures generated in the blast wave after jet impact further contribute to the overall depression in the solid.

While cavitation jets deforming and puncturing a material have been attributed as: (a) the cause of punctures in aluminium foil that has for decades been the favoured proxy used by industry to predict the cleaning potential of a given ultrasonic bath; (b) a possible way to inject drugs into tissue; and (c) the cause of pit formation in structures ranging from marine propellers to mercury containment facilities in pulsed neutron sources, there have never been any simulations showing this effect for the scenario of shock-induced bubble collapse. This numerical simulation work, to which this electronic supplement is part of, provides this. Furthermore, it provides methods for quantifying what bubble separations from the solid, bubble sizes, and pulse profiles might promote or inhibit erosion, as these cases (ranging from ship or nuclear to biomedical engineering) require.

The simulation work has been divided into 3 groups: (**1**) A single bubble of radius R_m = 40 μm attached to a rigid wall with bubble's centre separation distance from the wall of ξ = 0.95, 0.875, 0.75; (**2**) A single bubble R_m = 40 μm attached to an aluminium wall that is modelled as an elastic-plastic wall with three different separation distances (detached bubbles with $\xi > 1.0$, i.e. ξ = 2.0, 1.5, 1.25, 1.125; attached bubbles with $0 < \xi \leq 1.0$, i.e. ξ = 0.95, 0.875, 0.75, 0.5, 0.25; and attached bubbles with $\xi \leq 0$, i.e. ξ = 0, -0.25, -0.5); and (**3**) A single bubble R_m = 255 μm attached to a 25μm-thick aluminium foil with separation distance ξ = 0.95. The last one is done for a qualitative comparison with experiment. From these simulations, better insights and more meaningful conclusions were observed and drawn, i.e. whether the shock-bubble interaction would lead to the jetting collapse of the bubble or not, characteristics of the solid deformation (i.e. the crater and/or material depression), general flow physics surrounding the bubble and the toroidal bubble, and behaviour of shock-induced collapse of bubbles attached to a thin solid foil.

2. Free-Lagrange numerical scheme

Methodology

The free-Lagrange method (FLM) numerical code, *Vucalm*, solves the unsteady and compressible Euler equations in a Lagrangian reference frame. Currently, it can be used for 2D planar and axi-symmetric geometries. In contrast to conventional Lagrangian schemes, the mesh connectivity in the FLM is allowed to change freely in response to flow deformation. As a result, the mesh is immune to tangling, regardless of the degree of flow distortion. The absence of convective inter-cell fluxes results in minimal numerical diffusion of convected flow structures so that features such as material interfaces remain sharply resolved at all times. *Vucalm* was developed primarily for transient simulations involving compressible flows (Ball 1996). Further development has been incorporated into the code and now covers multi-phases (Ball *et al*. 2000; Howell & Ball 2000), the elastic-perfectly plastic response of solids subjected to extreme loading through the incorporation of elastic-plastic material models (Howell 2000; Howell & Ball 2002) and axisymmetric geometries (Turangan *et al*. 2008; Jamaluddin *et al*. 2011; Leighton *et al*. 2013). By incorporating these features within a single solver, we are able to illustrate the versatility of the technique for simulating highly transient and deforming multi-phase flows that involve extensive material distortion in solids.

The flow solver is based on a Godunov approach with nominal 2nd order accuracy in space and 1st order in time. The 2nd order spatial accuracy is achieved using a piecewise-linear reconstruction of the flow variables with a MUSCL-based slope limiter. Three types Riemann solvers adopted to FLM code are: the HLLC approximate solver by Toro *et al*. (1994) for air-air interfaces, the Riemann solver proposed by Flores & Holt (1981) for air-water and water-water interfaces, and the non-iterative approximate solver proposed by Dukowicz (1985) for solid-solid, solid-air and solid-water interfaces.

Riemann problem and the calculation of wave-processed variables

FLM is a particle method whereby each computational cell (control volume) encloses a single particle that is prescribed with a fluid or material type, time-dependent flow variables (e.g. density ρ, velocities (u, v) and temperature T (and stresses s if the simulations involve elastic-plastic solids)) and coordinates. The computational cells (and their particles) convect with local flow velocity. A Voronoi mesh is constructed based solely on the coordinates of the particles. In a Lagrangian frame, the cell boundary coincides with the contact surface of the local Riemann problem (the analogy of shock-tube diagram). All flow variables associated with the computational particles are extrapolated to their cell boundaries. These variables are then used for the calculation of the Riemann problem, for which the wave-processed variables (velocity u^*

and pressure p^*) are determined using the Riemann solvers. The details of how the Riemann problem is solved in *Vucalm* have been presented by Ball (1996).

Constitutive modelling

The constitutive modelling that describes how solid materials respond to loading used in the elastic-perfectly plastic model in our free-Lagrange (FLM) scheme is the elastic-perfectly plastic model whereby the von Mises yield condition implemented using the method of radial return is adopted. This approach, however, leads to some limitations of the model, as in practice solid materials do not yield with constant yield stresses and materials subjected to extreme loading will display many rate dependent effects (Howell & Ball 2002). The development of the material model and its incorporation into the FLM code, *Vucalm*, was not primarily intended to provide an extremely accurate tool for analysing large deformation problems in solid materials (i.e. high strain rate problems), but rather to demonstrate the adaptability of the free-Lagrangian and Riemann-based methods for arbitrary deformation finite volume schemes involving multi-phases.

Artificial surface tension (interface smoothing)

Particle methods, such as the FLM, suffer from some numerical instability associated with material interfaces. To alleviate this problem, a simple algorithm that functions like an artificial surface tension was developed and applied to particles located on dissimilar fluid interfaces (e.g. air-water, Ar-Xe and air-He interfaces) to smooth the interfaces (Howell & Ball 2000). The algorithm works by first identifying the particles that are located on the fluid interfaces. For a given "target" particle, its "interface neighbours" (located on fluid interfaces) are identified. A small restoring force is applied to the target particle so as to move it towards an imaginary line joining its neighbors. The algorithm helps to suppress the amplitude and growth rate of small scale perturbation of mesh-induced wavenumber instabilities on the interfaces. It was first tested and implemented in simulations of Richtmyer-Meshkov instability (see Howell & Ball 2000). For applications in the shock-induced bubble collapse, as discussed by Ball *et al*. (2000), Turangan *et al*. (2008), Jamaluddin *et al*. (2011) and Leighton *et al*. (2013), this artificial surface tension only affects the particle movement in localized regions around the interfaces. When coupling with fine-enough mesh resolution, the volumetric errors associated with the movement of the interface particles are negligible and that it does not affect the overall flow field under consideration. A parametric study associated with the strength of the restoring forces for the shock-induced bubble collapse simulation with bubble size of 40 μm and peak pressure of the shock of 60 MPa has been presented by Jamaluddin *et al*. (2011).

For the simulations of shock-induced bubble collapse involving elastic-plastic solids, the artificial surface tension is applied to air-water interfaces only because for solid materials, interface deformation is not influenced by these mesh-induced errors.

Equations of state (EOS)

The ideal gas equation of state (EOS) has been used to model air (i.e. $p = \rho RT$, where p is pressure, ρ is density, R = 287.14 J/kgK is the gas constant for air and T is temperature), and the Tait EOS for water (i.e. $p = B[(\rho / \rho_r)^\eta - 1]$, where ρ_r = 999.96 kg/m^3 is the reference density, and B = 3.31 x 10^8 Pa and η = 7 are constants). The application of these EOS in the present work is based on some assumptions. The following is quoted from Ball *et al*. (2000) regarding the application of the ideal (perfect) gas EOS in the context of the shock-induced bubble collapse (3mm-radius cylindrical bubble and 1.9 GPa shock):

> "The perfect gas equation of state is used in the air bubble for computational convenience. The magnitude of the errors incurred as a result of this choice can be estimated by comparing typical air temperatures from the simulation with values calculated using the Van der Waals equation, for the same pressure and density. At the time of liquid jet impact, the maximum pressure and temperature in the air cavity are approximately 35 MPa and 6000 K. At this condition, the perfect gas equation over-predicts the temperature by 150 K, or +2.6%. At the end of the simulation, the most extreme air state predicted is 300 MPa and 12000 K – in this case the error arising from the use of the perfect gas equation is 1400 K, or +13%. This source of error is, therefore, only really significant after jet impact, and never grows large enough to undermine the physical basis of the simulation. Dissociation of air has not been included. Taking the peak gas condition at jet impact (35 MPa and 6000 K), at equilibrium one would expect negligible nitrogen dissociation, and approximately 22% oxygen dissociation, giving a compressibility factor of 1.05. The impact of dissociation is therefore expected to be modest. At later times the degree of dissociation is expected to increase, but the shortage of equilibrium constant data above 6000 K makes this effect difficult to quantify."

Regarding the Tait EOS that is used to model the water phase, Ball *et al*. (2000) quoted:

> "Haas & Sturtevant (1987) argues that errors incurred by the use of the Tait equation become significant only when the liquid pressure exceeds 10 GPa. In the present work, the highest predicted pressure is approximately 5 GPa, which occurs briefly during the impact of the liquid jet on the bubble wall; the highest sustained pressure is the incident shock pressure of 1.9 GPa. We therefore conclude that the Tait equation is adequate for our purpose."

For solid materials, the Osborne EOS that takes the form of a quadratic fit to experimental data is also incorporated into *Vucalm* (see Howell & Ball (2002) for detailed formulation).

Limitations

Here, the heat and mass transfer, viscosity and surface tension have been omitted. For the shock-induced bubble collapse simulations, the temperature is calculated for the air phase only. This tends to over-estimate the prediction of temperature inside the bubble. We argue that the dynamics of the bubble is dominated by the water inertia and the timescale for the main events of the collapse is very short (i.e. < 0.3 μs, for the cases with 40 μm radius and shock strength of 60 MPa). The elastic-perfectly plastic model implemented using the method of radial return adopted here leads to some limitations of the model, as in practice solid materials do not yield with constant yield stresses and materials subjected to extreme loading will display many rate dependent effects. Therefore, the significant extra computational load taken to include these aspects was not, with current resources, considered commensurate with the extra accuracy they would bring. Additionally, owing to the formulation in 2D planar and axisymmetric geometries, the applications are limited to flow phenomena in those geometries, and that the 3D effects of the flow are not captured.

Validation

Vucalm has been validated numerous times against experiment and other numerical schemes. For shock-induced collapse, the work by Ball *et al*. (2000) is now treated as a benchmark for the shock-induced bubble collapse simulation – see Hawker & Ventikos (2012). The followings are some of the validation work performed to validate the code:

- Ball *et al*. (2000) simulated the collapse of a 3mm-radius cylindrical air cavity by a 1.9 GPa planar shock, and compared the results with the experiment conducted by Bourne & Field (1992).

- Turangan *et al*. (2008) simulated the shock-induced collapse of a 1mm-radius gas bubble in water by a 0.528 GPa planar shock. The result was compared with the simulation using the arbitrary Lagrangian-Eulerian (ALE) scheme by Ding & Gracewski (1996).
- Turangan *et al*. (2008) simulated the interaction of the 1.47-Mach shock wave with a cylindrical water column, and compared the results with the experiment by Igra & Takayama (1999).
- Related to simulations involving elastic-perfectly plastic material models, Howell & Ball (2002) has validated the code against fixed-connectivity Lagrangian and smooth-particle hydrodynamics (SPH) solvers for the simulations comprising the low-velocity impact of an aluminium projectile on a semi-infinite target, the collapse of a thick-walled beryllium cylinder and the high-velocity impact of cylindrical aluminium and steel projectiles on a thin aluminium target.

Recording of time histories of flow variables

In *Vucalm* simulations, each computational cell encloses a particle that is prescribed with a fluid or material type and time-dependent flow variables (ρ, (u, v), T, and stresses s if the simulations involve elastic-plastic solids). For each time step, the pressure of each particle is determined using the equation of state (EOS). As each particle is unique, it is straight forward to record the time histories of its pressure and flow variables. The method adopted to determine e.g. the peak pressure at the impact point of the jet when the jet hits the wall) is by identifying which particle ("target particle") that is located at this very specific location and who its immediate "neighbours" are. If pressure is or our interest, for every time step the pressure of this particle and its neighbours are averaged. The pressure-time history is then recorded in an output file that can be plotted (or extracted to get the peak pressure). Usually, the data are averaged from several computational particles (i.e. the target and the neighbours), depending on how fine the computational mesh is. Another approach is to pre-set the coordinates and radius of the pressure recording points. The particles that lie inside this radius are then identified and their values are recorded accordingly.

3. Shock-induced collapse of a single bubble attached to a wall

The FLM numerical code used in the present work introduced the ability to simulate the bubble response after the jet impacts the bubble's downstream wall, and so predicted the blast wave generated by this (Ball *et al*. 2000). This blast wave contained pressures far in excess of those which occur prior to the jet impact, and so FLM revealed and quantified what is probably the main damage mechanism for solids near such collapses. However, until this work, FLM could not predict damage from such collapses because it has not incorporated together multi-phases (Howell & Ball 2000, Ball *et al*. 2000), the elastic-perfectly plastic response of solids subjected to extreme loading through the incorporation of elastic-plastic material models (Howell 2000, Howell & Ball 2002) and axisymmetric geometry (Turangan *et al*. 2000; Jamaluddin *et al*. 2011; Leighton *et al*. 2013). This work incorporates these features within a single solver to illustrate the versatility of the technique for simulating highly transient and deforming multi-phase flows that involve extensive material distortion in solids. This work aims to allow damage predictions for applications ranging from erosion problems from a century ago (Brennen 1995) to modern ones in neutron generation facilities (Baik *et al*. 2010, Jiang *et al*. 2011, Leighton *et al*. 2012), and from opportunities in drug delivery (Ohl *et al*. 2003) to those in cleaning (Leighton *et al*. 2017), by simulating the shock-induced collapse of single bubbles attached to rigid and to elastic-plastic solid walls so as to examine the solid deformation associated with the jetting collapse of the bubbles for various scenarios.

Three groups of the simulations are presented:

- A single bubble of radius R_m = 40 μm attached to a rigid wall with bubble's centre separation distance from the wall of ξ = 0.95, 0.875, 0.75;
- A single bubble R_m = 40 μm attached to an aluminium wall that is modelled as an elastic-plastic wall with three different separation distances:
    - detached bubbles with $\xi > 1.0$, (i.e. ξ = 2.0, 1.5, 1.25, 1.125);
    - attached bubbles with $0 < \xi \leq 1.0$, (i.e. ξ = 0.95, 0.875, 0.75, 0.5, 0.25);
    - attached bubbles with $\xi \leq 0$, (i.e. ξ = 0, -0.25, -0.5);
- A single bubble R_m = 255 μm attached to a 25μm-thickness aluminium foil with separation distance ξ = 0.95. This case is intended for a qualitative comparison with an experiment of Philipp *et al*. (1993).

The comparison of the collapse of the bubble for three different distances (ξ = 0.95, 0.875, 0.75) for the case of bubble attached to a rigid wall is shown in **figure 1**. In **figure 2**, the parametric studies of a bubble attached to an aluminium wall for twelve different scenarios are presented. In **figure 3**, the collapse of a bubble attached to an aluminium foil is presented.

A **movie clip** showing the high speed jet impingement from the collapsing bubble for the case of a bubble attached to an aluminium wall with bubble radius R_m = 40 μm, separation distance ξ = 0.95 and lithotripter shock pressure of 60 MPa is available:
(*file name*: ShokcInducedCollapseAttachedToAluminiumWithSeparationDistance=0.95.wmv).

ζ = 0.950 **ζ = 0.875** **ζ = 0.750**

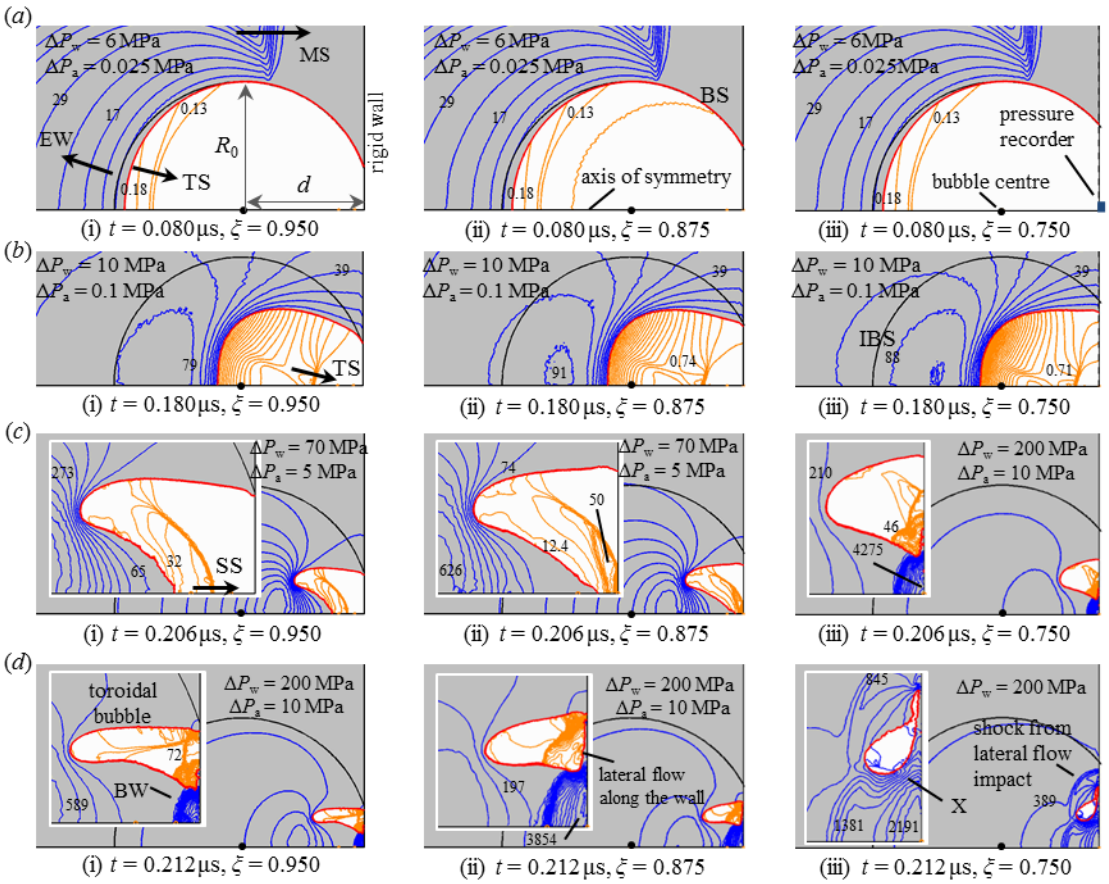

Figure 1: Comparison of the shock-induced collapse of a single bubble of radius R_0 = 40 μm initially attached to a rigid wall for three different separation distances d of the bubble's centre from the wall. The non-dimensional distances are $\xi = d/R_0 = \{0.95, 0.875, 0.75\}$. The radius of the fully spherical bubble R_0 is used as the scaling parameter. Insets are the close-up views. The unit of pressure contours is MPa. The labels are as follows: MS = Main lithotripter shock, EW = Expansion wave, TS = Transmitted shock, RS = Reflected shock, SS = Bow shock (in the bubble) and X = Pressure wave implosion. (Note: Figure 2 in the published article).

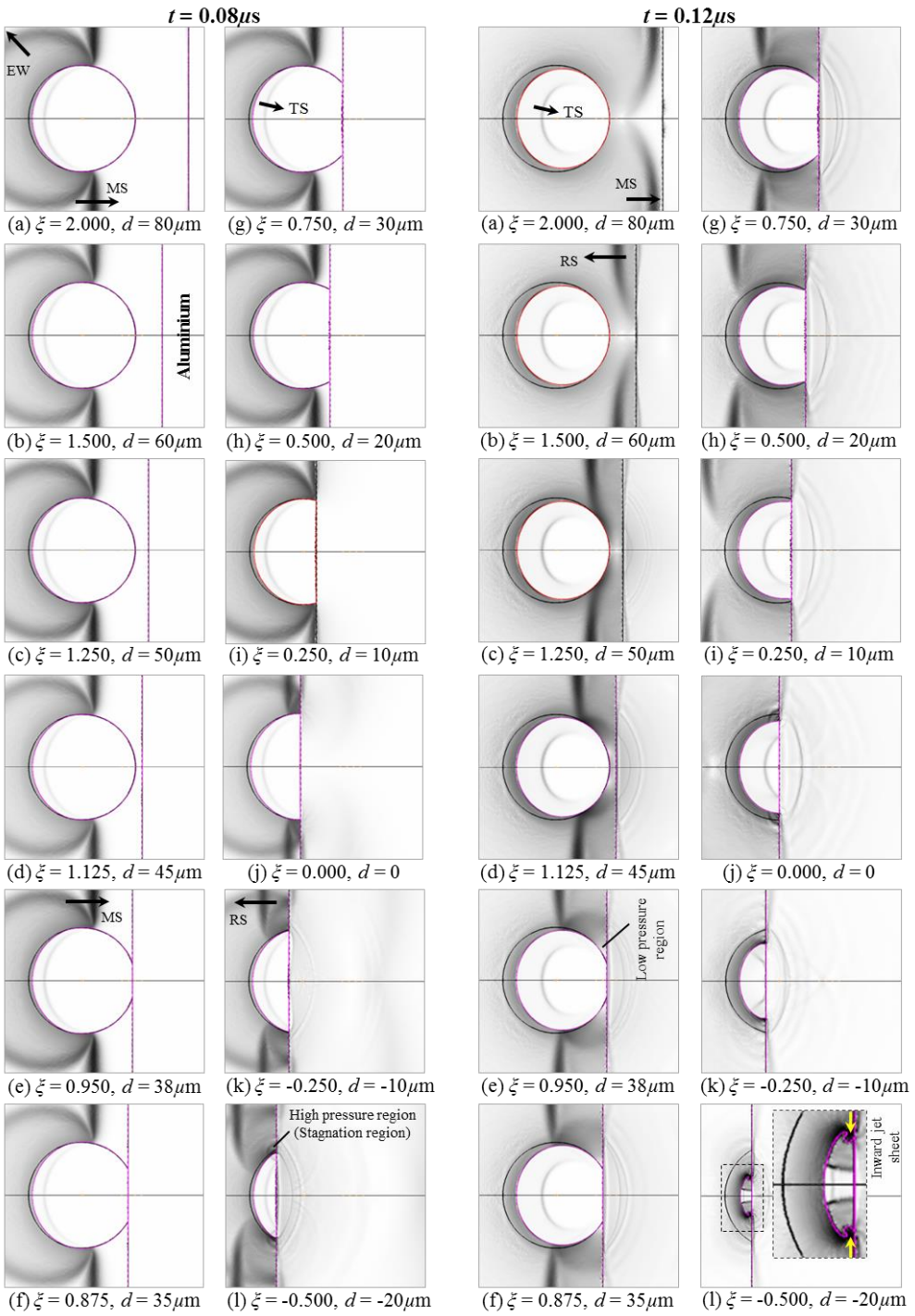

Figure 2: Schlieren-like plots showing the interaction of a lithotripter shock (P_s = 60 MPa) with stationary bubbles and the subsequent response of the bubbles that leads to their collapse at two different times from the shock initiation (t = 0.08 μs and t = 0.12 μs). A comparison of the shock-induced collapse of a single bubble (R_0 = 40 μm) initially attached to an aluminium wall (modelled as an elastic-plastic solid) for 12 different separation distances ξ. The non-dimensional distances are ξ = {2.0, 1.5, 1.25, 1.125} (for detached bubbles with $\xi > 1.0$), ξ = {0.95, 0.875, 0.75, 0.5, 0.25} (for attached bubbles with $0 < \xi \leq 1.0$) and ξ = {0, -0.25, -0.5} (for attached bubbles with $\xi \leq 0$).

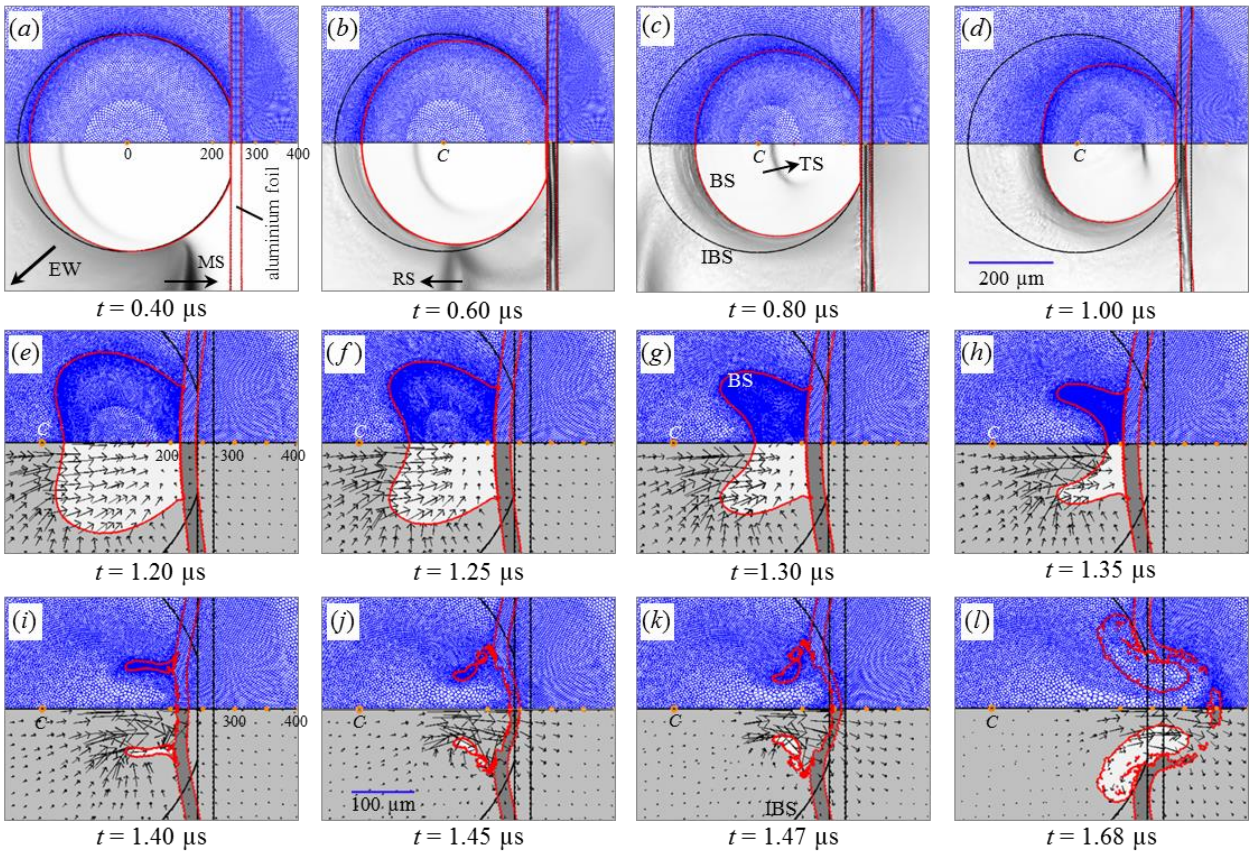

Figure 3: The plots of Voronoi mesh (top half) with Schlieren-like (bottom half) and Voronoi mesh with velocity vectors (bottom half) that show the interaction of the lithotripter shock wave with a single bubble attached to a 25 μm-thick aluminium foil. The foil tends to sway together with the flow but is eventually pierced by the high speed jet from the collapsing bubble when the "toroidal bubble" re-expands. The lithotripter shock has a peak pressure of $P_s \approx 65$ MPa. The bubble with initial radius $R_0 = 255$ μm is attached to the foil with a separation distance of $\xi = 0.95$. Frames (e) – (l) are close-up views. (Note: Figure 12 in the published article).

4. References

Baik K, Jiang J, Leighton TG. 2010 Acoustic attenuation, phase and group velocities in liquid-filled pipes: Theory, experiment, and examples of water and mercury. *J. Acoust. Soc. Am.* **128**(5), 2610–2624 (doi: 10.1121/1.3495943).

Ball GJ. 1996AFree-Lagrange method for unsteady compressible flow: simulation of a confined cylindrical blast wave. *Shock Waves* **5**, 311–325.

Ball GJ, Howell BP, Leighton TG, Schofield MJ. 2000 Shock-induced collapse of a cylindrical air cavity in water: a Free-Lagrange simulation. *Shock Waves* **10**, 265–276.

Bourne NK, Field JE. 1992 Shock-induced collapse of single cavities in liquids. J. Fluid Mech. **244**, 225–240.

Brennen CE. 1995. Cavitation and Bubble Dynamics. *Oxford University Press*.

Ding Z, Gracewski SM. 1996 The behaviour of a gas cavity impacted by a weak or strong shock wave. *J. Fluid Mech*. 309, 183–209.

Dukowicz JK. 1985 A general, non-iterative Riemann solver for Godunov's method. *J. Comput. Phys*. 61, 119–137.

Flores J, Holt M. 1981 Glimm's method applied to underwater explosions. *J. Comput. Phys*. 44, 377–387.

Haas J-F, Sturtevant B. 1987 Interaction of weak shock waves with cylindrical and spherical inhomogeneities. *J. Fluid Mech*. **181**, 41–76.

Hawker NA, Ventikos Y. 2012 Interaction of a strong shockwave with a gas bubble in a liquid medium: a numerical study. *J. Fluid Mech*. **132**, 1–39.

Howell BP. 2000 An investigation of Lagrangian Riemann methods incorporating material strength. *PhD Thesis*, University of Southampton, UK.

Howell BP, Ball GJ. 2000 Damping of mesh-induced errors in free-Lagrange simulations of Richtmyer-Meshkov instability. *Shock Waves* **10**, 253–264.

Howell BP, Ball GJ. 2002 A free-Lagrange augmented Godunov method for the simulation of elastic-plastic solids. *J. Comput. Phys*. **175**, 128–167.

Igra D, Takayama K. 1999 Investigations of aerodynamic breakup of a cylindrical water droplet. *Tech. Rep. 11*. Institute of Fluid Science, Tohoku University, Japan.

Jamaluddin AR, Ball GJ, Turangan CK, Leighton TG. 2011 The collapse of single bubbles an approximation of the far field acoustic emissions for cavitation induced by shock wave lithotripsy. *J. Fluid Mech*. **677**, 305–341.

Jiang J, Baik K, Leighton TG. 2011 Acoustic attenuation, phase and group velocities in liquid-filled pipes II: Simulation for spallation neutron sources and planetary exploration. *J. Acoust. Soc. Am.* **130**(2), 695–706 (doi:10.1121/1.3598463).

Leighton TG, Baik K, Jiang J. 2012 The use of acoustic inversion to estimate the bubble size distribution in pipelines. *Proc. Royal Soc. A* **468**, 2461–2484 (doi:10.1098/rspa.2012.0053).

Leighton TG, Turangan CK, Jamaluddin AR, Ball GJ, White PR. 2013 Prediction of far-field acoustic emissions from cavitation clouds during shock wave lithotripsy for development of a clinical device. *Proc. Roy. Soc. A* **469**, 21pp, doi: 10.1098/rspa.2012.0538.

Leighton TG. 2017 The acoustic bubble: Ocean, cetacean and extraterrestrial acoustics, and cold water cleaning. *IOP J. of Phys.: Conference Series* 797, 012001.

Ohl CD, Ikink R. 2003 Shock-wave-induced jetting of micron-size bubbles. *Phys. Rev. Lett*. **21**, 214502.

Philipp A, Delius M, Scheffczyk C, Vogel A, Lauterborn W. 1993 Interaction of lithotripter-generated shock waves with air bubbles. J. Acoust. Soc. Am. 93(5), 2496–2509.

Toro EF, Spruce M, Speares W. 1994 Restoration of the contact surface in the HLL-Riemann solver. *Shock Waves* 4, 25–34.

Turangan CK, Jamaluddin AR, Ball GJ, Leighton TG. 2008 Free-Lagrange simulations of the expansion and jetting collapse of air bubbles in water. *J. Fluid Mech*. **598**, 1–25.